FATIGUE LIFE IMPROVEMENT OF AN ALUMINUM ALLOY FSW WITH LOW PLASTICITY BURNISHING

N. Jayaraman, P. Prevéy, and M. Mahoney

Abstract

Friction stir welding provides a new technology for solid state joining of a wide variety of aluminum alloys that cannot be joined with conventional fusion welds. However, recent work has shown that significant tensile residual stresses are developed in the stirred region with local tension maxima at the transition between the stir and heat-affected zones. Residual tension at the edges of the stir zone has been associated with stress corrosion cracking and corrosion fatigue crack growth initiation. This fatigue debit has been overcome using low plasticity burnishing (LPB) to introduce a deep surface layer of compressive residual stress. LPB processing after friction stir welding has increased the high cycle fatigue endurance of aluminum alloy FSW by 80%. However, the LPB processing parameters have not yet been optimized to produce the maximum achievable fatigue life.

A linear elastic fracture mechanics approach is applied to calculate the fatigue crack growth rates and fatigue lives of friction stir welded 2219-T8751 aluminum with initiation from salt fog pitting. The analysis is performed with and without the including of the deep compressive residual stresses produced by low plasticity burnishing (LPB). Calculated fatigue lives are compared to fatigue data developed in four-point bending at R = 0.1 following 100 hr. salt fog pitting corrosion. The results indicate that the improved fatigue life achieved with LPB after friction stir welding can be explained by delayed crack initiation and retardation of growth in the deep compressive layer produced by LPB. The fatigue crack growth analysis provides a theoretical basis for understanding the improved fatigue life realized with LPB and for estimating the residual stress distribution that will provide the highest achievable fatigue strength.

Introduction

A new surface enhancement technology has been developed which can provide compression in the surface layer of sufficient depth to effectively eliminate the degradation in corrosion fatigue life attributed to salt pit corrosion. Low plasticity burnishing (LPB)[1-5,] has been demonstrated to provide deep and high magnitude compression. CNC tools can be used to apply the process at costs and speeds comparable to conventional machining operations.

Salt spray corrosion pits are a common site of fatigue crack initiation in aluminum alloy structures. Salt corrosion pitting occurs during exposure to a marine atmosphere and results in intergranular corrosion to a depth depending on the time of exposure, temperature, and the service environment. The pronounced fatigue strength reduction caused by salt pit corrosion is well established for both steels[6] and aluminum

Proceedings 132nd TMS Annual Meeting
March 2-6, 2003, San Diego, CA

alloys,[7] and typically reduces the endurance limit to nominally half of the uncorroded value.

Recent preliminary studies[2] on salt spray corroded 7075-T6 aluminum have demonstrated full restoration of the original material endurance limit and a 10x increase in life in the finite fatigue life range. Studies on LPB processed 7050-T7651 FSW samples show a nominal 60% increase in endurance limit due to the LPB treatment.

Friction stir welding (FSW) is a new solid state joining process for aluminum alloys including those alloys considered not weldable. However, the FSW process produces zones of tensile residual stress at the edges of the stir zone. Recent residual stress studies performed at Lambda Research on aluminum and titanium alloy FSW samples show tensile residual stresses throughout the weld thickness with maximum tension near the weld edges. Pitting and stress corrosion cracking has been observed to follow these regions of tension in aluminum welds. Also, the surface finish produced by FSW, although relatively flat, is not adequate for many applications.

LPB offers the opportunity to induce a layer of compressive residual stress into the weld surface, heat affected zone (HAZ), and adjacent parent metal while smoothing the weld crown. Residual stresses in FSW samples before and after LPB will be shown. High cycle fatigue data, both empirical and predicted, showing the effect of LPB on fatigue performance will also be shown.

Experimental Technique

Material

Material used in this study was 2219-T8751 aluminum friction stir welded plates with nominal composition 6.3Cu – 0.3Mn – 0.2Si – 0.3Fe – 0.1Zn - 0.02Mg – 0.06Ti – Remainder Al. Nominal dimensions of the plates were 914 (length) x 152 (width) x 9.5mm (thick). The plates contained a single weld in the center down the 914 mm length.

Low Plasticity Burnishing

LPB produces a layer of compressive residual stress of high magnitude and depth with minimal cold work.[1-5] It is usually performed using a single pass of a smooth free rolling ball under a normal force sufficient to plastically deform the surface of the material. Hertzian loading creates a layer of compressive residual stress to a depth as much as 4 mm. The ball is supported in a fluid bearing with sufficient pressure to lift the ball off the surface of the retaining spherical socket. The ball is in solid contact only with the surface to be burnished, and is free to roll on the surface of the work piece. LPB was optimized for the 2219-T8751 friction stir weld. Optimal LPB parameters were developed to impart the greatest depth and magnitude of residual stress with minimal cold work.

For this work, the LPB was performed in the direction of the weld using multiple passes adjacent to and in the weld. LPB pressure was controlled to develop the desired magnitude and depth of compressive stress with relatively low cold working. Figure 1 shows a friction stir weld in the process of being low plasticity burnished on a CNC milling machine.

High Cycle Fatigue Testing

All high cycle fatigue tests were performed under constant stress amplitude load at ambient temperature in four-point bending on a Sonntag SF-1U fatigue machine. A photo of the fatigue test setup is shown in

Figure 2. The cyclic frequency and load ratio, R, were 30 Hz and 0.1, respectively.

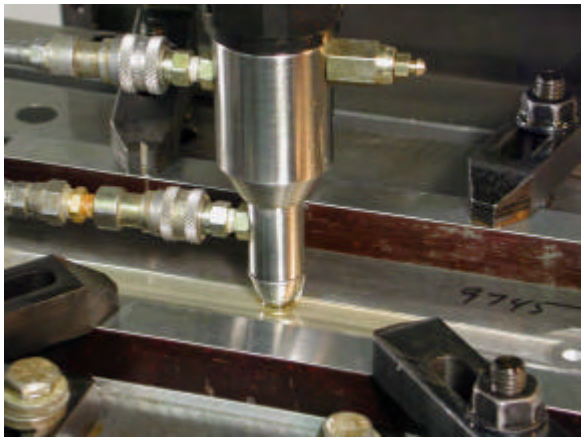

Figure 1: Photo of friction stir welded plate being low plasticity burnished with single ball tool.

Tests were conducted to specimen fracture or until a "run-out" life of 2 x 10^6 was attained, whichever occurred first. "Run-out" specimens were subsequently fatigue re-tested to fracture at 20 ksi or greater max stress above the stress level at which "run-out" had occurred. For analysis purposes, such re-tests were regarded as virgin tests, and were included in the S-N results.

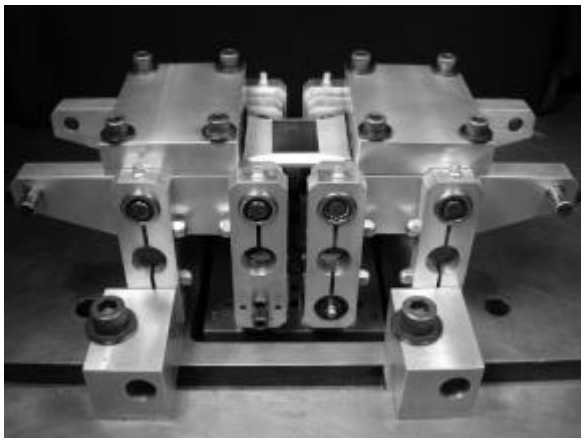

Figure 2: Photo of LPB friction stir welded fatigue specimen in 4-point bend fatigue fixture.

A fatigue sample with a trapezoidal gage cross-section shown in Figure 3 was used for the HCF testing. The trapezoidal cross-section HCF sample was designed to force fatigue failures to initiate in the compressive gage section. The sample, shown in Figure 3, features 30-deg. sloping sides that could be burnished, shot peened, or otherwise surface enhanced along with the top test surface of the gage section. The region of uniform high compression then extends from the test surface to below the neutral axis in bending on both sides of the sample when under load. By developing deep compression down the sides of the sample, as well as on the more highly stressed test surface, fatigue failure will initiate from the top surface.

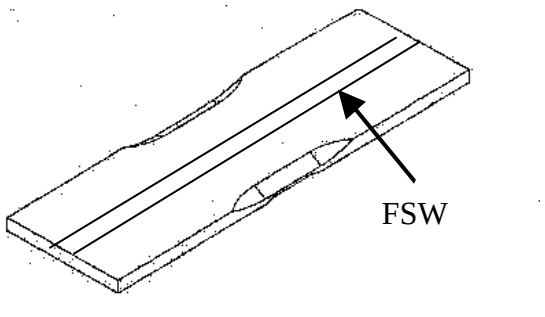

Figure 3: Trapezoid fatigue sample manufactured from FSW plate specimens.

All HCF samples were milled on the weld side prior to LPB or salt fog exposure to remove the weld flash and circular grooves left by the FSW process. The weld flash was milled flush with the parent metal. A total of four S-N curves were generated from the following groups of specimens:

Group No.	Group Identification
1	As-Welded + Milled
2	As-Welded + Milled + LPB
3	As-Welded + Milled + 100 hr. Salt Exposure
4	As-Welded + Milled + LPB + 100 hr. Salt Exposure

Following fatigue testing, each specimen was examined optically at magnifications up to 40X to identify fatigue origins and locations

thereof relative to the specimen geometry. Photographs of the fracture faces were taken with a Nikon 990 digital camera through a stereoscope microscope at 15X.

Fatigue Modeling

Fatigue life-prediction modeling analysis was performed using a fatigue crack growth prediction model based on linear elastic fracture mechanics. The crack growth conditions on the trapezoidal bar geometry (Figure 3) were simulated using a rectangular cross-section bar of width 1 in. and thickness 0.25 in. with a center surface flaw subjected to 4-point bending fatigue conditions. The general procedure involved assuming a starting semi-circular surface flaw and computing the crack growth conditions cycle-by-cycle up to the point of failure. In this analysis, a starting flaw size was chosen for each condition such that the endurance limit and HCF behavior were most accurately predicted. Failure condition was achieved when Kmax > Kc or net section stress (Snet) > Y.S. or when the crack reached the side surface or bottom surface of the rectangular bar. A crack growth prediction computer code developed at Lambda Research was used to perform these calculations. The fatigue crack growth was followed using the following Forman fatigue crack growth expression:[8]

Forman equation – $da/dN = C_2 (\Delta K)^{m2} / [(1-R)K_c - \Delta K]$

$= C_2 (\Delta K)^{m2} / [(1-R)(K_c - K_{max}]$

where C_2 and m2 are Forman constants.

K-solutions for a semi-circular surface center crack for pure bending condition was obtained from ref (9).

$K_I = (\sigma_m + H \sigma_b) \sqrt{\pi a/Q} F(a/t, a/c, c/W, \phi)$ … Eq. (2)

Where σ_m is the axial stress on the bar normal to the crack plane

σ_b is the bending stress on the bar

a and c are the crack depth and length, respectively

H, Q, and F(a/t, a/c, c/W, ϕ) are geometrical factors

The specimens in this program were subjected to pure bending forces. Appropriate corrections were made to the bending stresses using the residual stress profiles from Figure 4f. In the case of LPB treatment, the small starting crack grew into the compressive residual stress field whereby the effective stress intensity at the crack tip was reduced substantially – this in turn resulted in grossly reduced crack growth rates. Additionally, since the residual stresses are different near the surface as compared to the gradient through the depth, the crack shape which was assumed to be semi circular invariably assumed an elliptical shape as it progressed through the compressive residual stress zone.

Full S-N curves were predicted using these test conditions and these predictions were compared with actual fatigue life of tested specimens. The following material property data was used in making these predictions:

Y.S. = 365 MPa (53 ksi), E = 73 Gpa, ν (Poisson's ratio) = 0.3 (10,600 ksi), K_{IC} = 36 MPa $\sqrt{m}$ (33 ksi $\sqrt{in}$), and
K_C = 72 MPa $\sqrt{m}$ (66 ksi $\sqrt{in}$),
Forman constants: m2 = 3.77 and
C2 = $1.27(10^{-6})$(mm/cycle)/(MPa $\sqrt{m}$)^{m2} = $(6.39(10^{-8})$ in/cycle/(ksi $\sqrt{in}$)^{m2} and

Corrosion Exposure

Prior to fatigue testing, the as welded + milled and as welded + milled + LPB test specimens were exposed to a 5 percent (by weight) NaCl solution fog at a temperature

of 95F for 100 hrs. The exposure was performed in a Singleton Salt Fog Cabinet in accordance with ASTM Specification B117-97.

Hardness Determination

Hardness measurements were made at the surface of an as welded + milled fatigue specimen. Measurements were made as a function of distance from the weld both in the parent metal and in the weld. A Wilson Rockwell hardness tester was used for the measurements.

Residual Stress Measurements

Residual stress distributions were measured for an as welded + milled and as-welded + milled + LPB sample using an automated translation device, capable of collecting a large volume of measurements in a relatively small amount of time, with minimal technician interaction.[10] X-ray diffraction residual stress measurements were made at the weld (top) surface, at 1/4, 1/2 and 3/4 thickness, and the root (bottom) surface. Measurements were made parallel and perpendicular to the weld-line at all five depths and as a function of distance from the weld center in ~2.5mm steps. Only the weld side of the sample was LPB processed over a 2.0-in wide zone centered on the weld thus including the HAZ.

XRD residual stress measurements were made employing a $\sin^2\psi$ technique and the diffraction of chromium $K\alpha_1$ radiation from the (311) planes of the 2219-T8751. It was first verified that the lattice spacing was a linear function of $\sin^2\psi$ as required for the plane stress linear elastic residual stress model.[11-14] The samples were rocked through an angular range of ±1.5º around the mean psi angles during measurement to integrate the diffracted intensity over more grains in order to minimize the influence of the grain size.

Measurements were made below the surface by electropolishing to each depth. The residual stress measurements were corrected for both the penetration of the radiation into the subsurface stress gradient[15] and for stress relaxation caused by layer removal.[16]

The value of the x-ray elastic constants required to calculate the macroscopic residual stress from the strain normal to the (311) planes of the 2219-T8751 were determined in accordance with ASTM E1426-91.[17] Systematic errors were monitored per ASTM specification E915.

Results and Discussion

Residual Stresses

The residual stress distributions measured as functions of depth and distance from the weld centerline are presented in Figures 4a-4e. Each plot presents residual stresses parallel and perpendicular to the weld line for a given depth through the thickness of the plate in ¼ thickness increments. On the weld surface and root surface, residual stresses were also measured in the 45° direction. Compressive stresses are shown as negative values and tensile as positive.

At the weld surface, the as-welded samples are in tension in the parallel direction and compression in the perpendicular direction. Following LPB, the residual stress is compressive in all directions, ranging from –180 to –500 MPa at the weld surface.

Residual stresses vary as a function of distance from the weld centerline, reaching minimums in the regions that correspond to the HAZ's on both the advancing and retreating sides. This is likely due to the LPB procedure. In this study, no attempt was made to adjust the burnishing load to

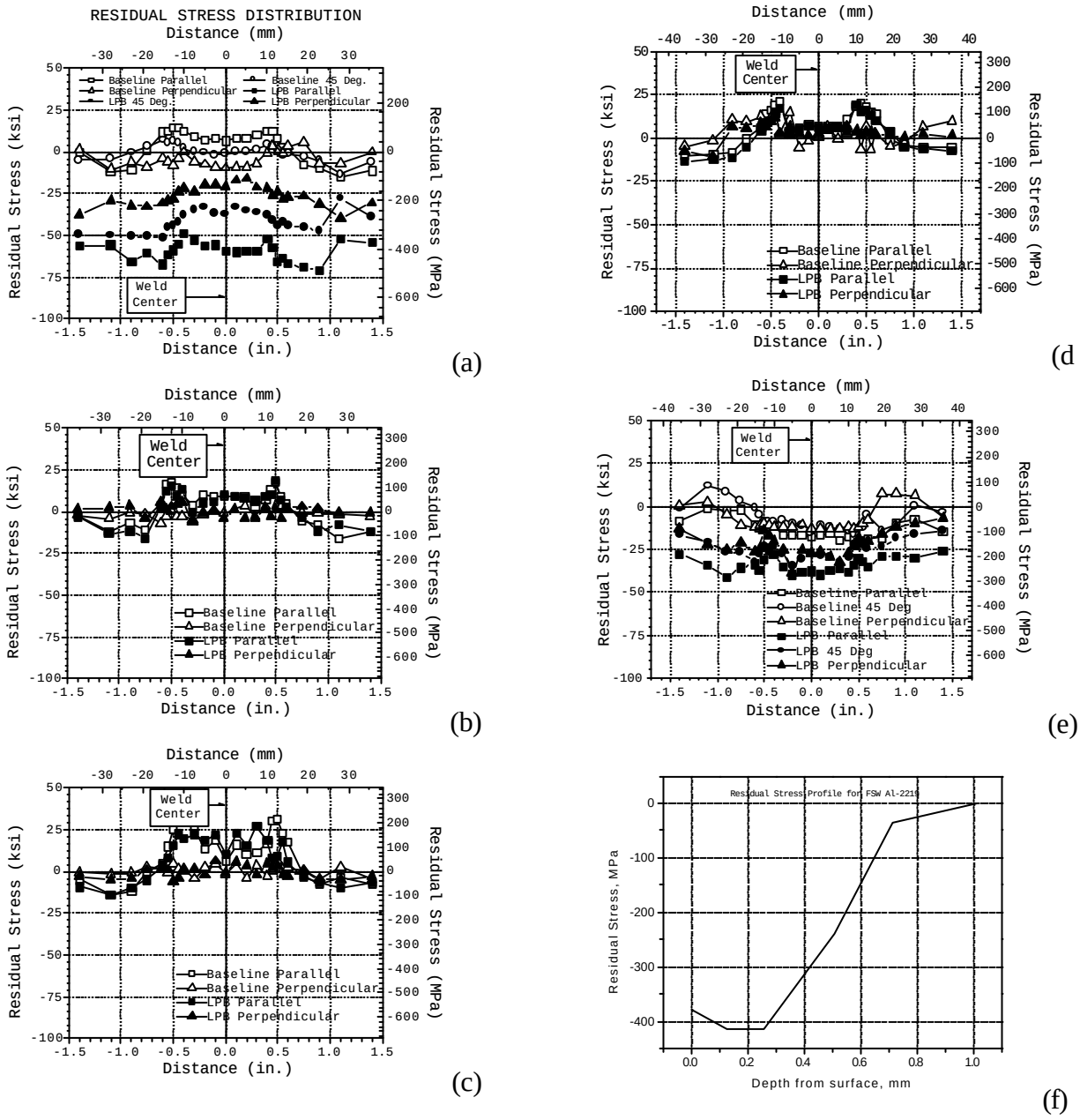

Figure 4: Residual stress measurements in FSW 2219 T8751 aluminum with and without low plasticity burnishing, (a) weld surface, (b) ¼ thickness, (c) ½ thickness, (d) ¾ thickness, (e) weld root surface, and (f) residual stress depth profile from surface

the yield stress of the 2219 Al. Thus, in the softer HAZ's, the response to the LPB would be different than that in the higher yield stress weld zone and parent metal.

At ¼, ½, and ¾ thickness the as welded and LPB samples have similar residual stress patterns, Figs. 4b-4d. The influence of LPB was limited to a depth of less than 1/4 thickness in order to minimize distortion. The results for both samples show an increase in tensile residual stresses in the parallel direction at mid-thickness. Tensile stresses are highest near the weld edges and approach +240 MPa. These are much higher values than reported previously where measurements

were taken only near the crown and not at the root.[18] Residual stresses perpendicular to the weld direction are essentially zero.

Figure 4e illustrates residual stresses on the weld root surface. For the as-welded sample within the weld zone, residual stresses are compressive and relatively low at approximately -100MPa in the parallel, 45°, and perpendicular directions. Following LPB, these stresses become more compressive ranging from -20 to –250MPa. Although only the top surface was treated by LPB, the bottom surface experiences compression due to plate bending.

Hardness Determination

Surface hardness measurements, made on an as welded + milled specimen are shown in Figure 5. The measurements are shown on a Rockwell B scale as a function of distance from the weld center. The results indicate relatively soft material in the weld as compared to the parent material. The softest material is located near the edges of the weld.

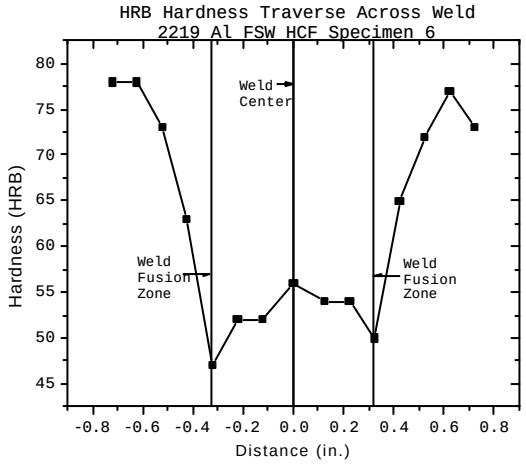

Figure 5: Surface hardness traverse on milled fatigue specimen showing softened weld material.

Fatigue and Corrosion Fatigue

High cycle fatigue results are presented in Figure 6 for the different test conditions. For FSW material, with the flash and circular tool pattern removed by milling, the endurance limit was nominally 230MPa. The endurance limit for the milled specimens was decreased by nominally 25% after the 100 hr salt exposure. LPB of the milled samples increased the endurance limit to 300MPa. The 100 hr. salt exposure had little influence on the fatigue strength of the LPB specimens.

Fatigue initiation sites for the milled specimens were typically at the surface within the gage region. An example of a surface initiation is shown in the photo in Figure 7. Specimens that were cycled at higher maximum stresses had multiple initiations, but within the gage. Almost all the initiation sites were outside of the weld material. LPB moved the fatigue initiation site from the surface of the gage section to the corners as shown in Figure 8. At low stresses, crack initiation was located subsurface at the corners. An example of a subsurface initiation is shown in Figure 9. Subsurface initiations, originating below the highly compressive surface, do not effectively demonstrate the full effect of LPB processing on fatigue performance. Presumably, an even higher applied stress would have been required to initiate failure from the surface. However, the occurrence of failures below the LPB compressive layer reveals the substantial fatigue enhancement benefits of LPB.

Fatigue initiation sites for salt corroded specimens were comparable to that for samples not corroded. However, the corroded bars exhibited more multiple initiation sites as a result of numerous corrosion pits, especially for the milled + 100 hr salt specimens. Figure 10 shows a surface failure from a corrosion pit for a milled + 100 hr salt sample. Samples treated via LPB prior to corroding failed from

the specimen corner and not from the corrosion pits. LPB was effective in preventing the corrosion pits from acting as fatigue initiation sites.

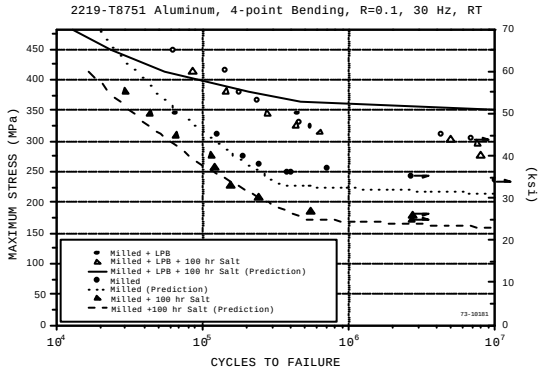

Figure 6 - Fatigue and corrosion/fatigue test results for friction stir welded 2219-T8751 aluminum with and without low plasticity burnishing.

Figure 7: Fracture face showing typical surface failure for milled specimen.

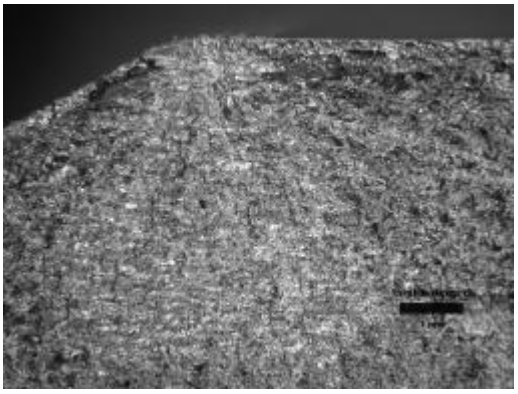

Figure 8: Fracture face showing typical corner failure for LPB specimen.

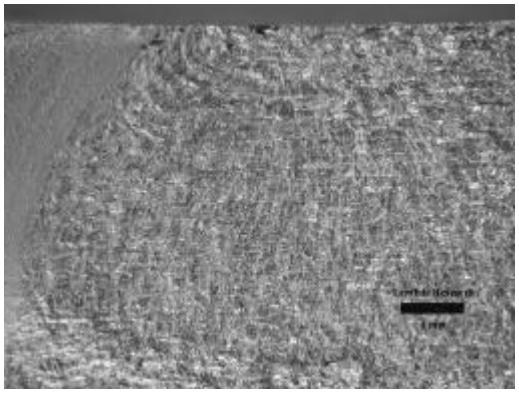

Figure 9: Fracture face showing subsurface initiation in LPB specimen.

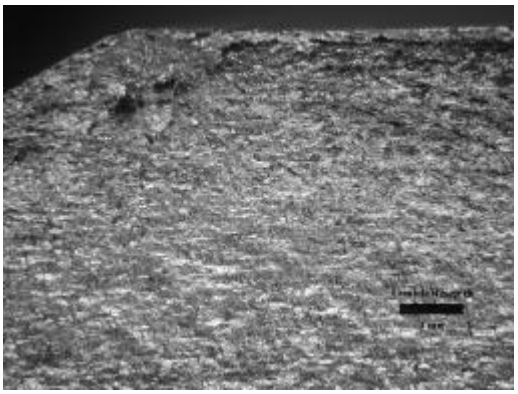

Figure 10: Fracture face for Milled + 100 hr. Salt Exposure specimen showing surface initiation at corrosion pit adjacent to weld.

Fatigue Modeling

Figure 6 shows a comparison of test results of test specimens and S-N curves generated from the life prediction analysis. Generally for the as-milled specimens and milled specimens exposed to 100 hrs of salt, the predicted S-N curves gave reasonable validation of test results. As seen in this plot, the HCF life predictions for the as-milled condition and the milled + 100 hr salt exposure conditions were excellent.

The results for specimens with surfaces treated with the LPB process were quite different; both in the LPB processed conditions and LPB + 100 hrs salt exposure

conditions, the predictions were consistently higher than the test results. In fact, the predictions for the LPB processed condition were so high that those are not even presented in this figure and the ones for LPB + 100 hrs salt exposure is clearly higher than the test results. Another clear observation from Figure 6 is that while the as-milled and milled + 100 hrs salt exposure conditions showed significant differences in fatigue life performance (both in fatigue life at the same stress level and in the corresponding fatigue strengths), the results for the LPB processed and LPB + 100 hrs of salt exposure conditions are almost indistinguishable. Coincidentally, most test specimens under these test conditions showed sub-surface crack initiation, thus making the effect of corrosion irrelevant in the analysis. A more accurate life-prediction methodology incorporating sub-surface cracking mechanisms is needed to fully and more accurately predict fatigue life. This is currently being completed in an in-house research program at Lambda Research.

Conclusions

- LPB was shown to produce high compressive residual stresses in 2219-T8751 aluminum friction stir welds. LPB was performed using conventional CNC machine tools at costs and speeds comparable to conventional machining operations.
- The As-welded samples had tensile residual stresses greater than +200 MPa in the direction parallel to the weld line. After LPB the surface of the FSW specimen was in compression, as high as –450 MPa, in all directions.
- LPB increased the endurance limit by nominally 60% in salt corroded FSW specimens. Specimens that were LPB and salt corroded had the same nominal fatigue strength as samples that were LPB processed without corrosion indicating the LPB process eliminated any fatigue debit from salt fog corrosion.
- Fatigue failures for some LPB samples initiated below the surface. The occurrence of failures below the LPB compressive layer demonstrates the dramatic fatigue enhancement associated with LPB.

Acknowledgment

The authors gratefully acknowledge Boeing for financial support.

References

1 P. Prevéy, et.al. “FOD Resistance and Fatigue Crack Arrest in Low Plasticity Burnished IN718,” Proceedings of the 5th National High Cycle Fatigue Conference, (2000).

2 J. Cammett and P. Prevéy, “Low Cost Corrosion Damage Mitigation and Improved Fatigue Performance of Low Plasticity Burnished 7075-T6,” Proceedings of the 4th International Aircraft Corrosion Workshop, Solomons, MD, Aug. 22-25, (2000).

3 P. Prevéy, et.al., “The Effect of Low Plasticity Burnishing (LPB) on the HCF Performance and FOD Resistance of Ti-6Al-4V,” Proceedings 6th National Turbine Engine HCF Conference, Jacksonville, FL, March 5-8, (2001)

4 J. Cammett and P. Prevéy, “Fatigue Strength Restoration in Corrosion Pitted 4340 Alloy Steel via Low Plasticity Burnishing,” Retrieved Aug. 30, 2002, from http://www.lambda-research.com/publics.htm.

5 P. Prevéy and J. Cammett, “The Influence of Surface Enhancement by Low Plasticity Burnishing on the Corrosion Fatigue Performance of AA7075-T6,” Proceedings 5th International Aircraft Corrosion Workshop, Solomons, MD., Aug. 20-23, (2002).

6 ASM Handbook, Vol. 19, Fatigue and Fracture, S.R. Lampman, ed., ASM International, Metals Park, OH, 1996, pp. 596-597.

7 N.E. Dowling, Mechanical Behavior of Materials, Prentice Hall, NJ, (1993) p. 365.

8 D. Broek, Elementary Engineering Fracture Mechanics, Martinus Nijhoff Publishers, Dordrecht., 1987, p. 264.

9 T.L. Anderson, Fracture Mechanics – Fundamentals and Applications, CRC Press, Boca Raton, 1995, P627.
10 Diffraction Notes, Residual Stress Contour Mapping, (No. 19, Summer 1997)
11 M. Hilley ed., Residual Stress Measurement by X-Ray Diffraction, *SAE J784a*, (Warrendale, PA: Society of Auto. Eng.), (1971)
12 I. Noyan, and J. Cohen, Residual Stress Measurement by Diffraction and Interpretation, (New York, NY: Springer-Verlag), (1987).
13 B.D. Cullity, Elements of X-ray Diffraction, 2nd Ed., (Reading, MA: Addison-Wesley), (1978) p 447-476.
14 P. Prevéy, "X-ray Diffraction Residual Stress Techniques," Metals Handbook, **10**, (Metals Park, OH: ASM), (1978) p 380-392.
15 D.P. Koistinen and R.E. Marburger, Transactions of the ASM, (1964), **67**.
16 M.G. Moore and W.P. Evans, "Mathematical Correction for Stress in Removed Layers in X-ray Diffraction Residual Stress Analysis," *SAE Transactions*, **66**, (1958), p 340-345.
17 P. Prevéy, "A Method of Determining Elastic Properties of Alloys in Selected Crystallographic Directions for X-ray Diffraction Residual Stress Measurement," Adv. In X-ray Analysis , **20**, (New York, NY: Plenum Press) (1977), p 345-354.
18 M. James, M. Mahoney and D. Waldron, Proceedings of the 1st International Symposium on Friction Stir Welding, Rockwell Science Center, T.O., CA, Pub. By TWI, June 14-16, (1999).